Journal of Engineering and Sustainable Development
Vol. 29, No. 04, July 2025
https://jeasd.uomustansiriyah.edu.iq/index.php/jeasd
ISSN 2520-0917
Research Article
https://doi.org/10.31272/jeasd.2877

Photocatalytic CO_2 Conversion with H_2O to CO and CH_4 Over V_2C/TiO_2 Composite

Beenish Tahir[1], Mustafa Jawad Nuhma[2], Muhammad Tahir[1*], Abdulrahman Alraeesi[1], Ali A. Jazie[2], Naveen Kumar[3]

[1]Chemical and Petroleum Engineering Department, UAE University, P.O. Box 15551, Al Ain, United Arab Emirates
[2]Chemical Engineering Department, College of Engineering, University of Al-Qadisiyah, Al-Diwaniyah City 999048, Iraq
[3]Department of Chemistry, Maharshi Dayanand University, Rohtak, 124001, India

[*]Email: muhammad.tahir@uaeu.ac.ae

Article Info

Received	**23/07/2024**
Revised	**01/02/2025**
Accepted	**25/02/2025**

Abstract

Photocatalytic reduction of CO_2 to valuable chemicals and fuels requires highly efficient semiconductor materials, and most available photocatalysts are less efficient. Due to their unique electrical properties, the new family of two-dimensional materials known as MXenes has drawn much interest in photocatalytic applications. The vanadium carbide (V_2C) is one of the significant MXenes being considered because of its many advantages over other materials. In this work, V_2C-loaded TiO_2 composites were synthesized and tested for photocatalytic reduction of CO_2 with H_2O to produce value-added CO and CH_4 fuels in a continuous flow photoreactor system. The optimized 10 % V_2C-TiO_2 was responsible for CO and CH_4 formation of 1233.8 and 85.2 µmol g^{-1} h^{-1}, respectively, which were many-fold higher than using pure TiO_2. This enhanced photoactivity of the composite was due to increased conductivity, many active sites, and higher light absorbance, which allowed for the efficient separation of charge carriers and light absorbance. Thus, MXenes, particularly 2D V_2C MXene, would be a promising cocatalyst to combine with a semiconductor to maximize photocatalytic activity during CO_2 reduction application.

Keywords: Cocatalyst; Conversion; Photoactivity; Titanium Dioxide; Vanadium Carbide MXene

1. Introduction

The massive greenhouse gas carbon dioxide (CO_2) emission from fossil fuel combustion and human activities is responsible for global warming. Recycling CO_2 through green and sustainable processes to generate value-added products like methane (CH_4), carbon monoxide (CO), and methanol (CH_3OH) is one of the key tactics to lessen the greenhouse effect. Among the various technologies, the photocatalytic CO_2 reduction reaction (PCO_2R) with the use of solar energy is promising to achieve sustainable development goals (SDGs), given the renewable energy strategy and climate action [1]. This approach of CO_2 reduction through photocatalysis will lower CO_2 levels in the atmosphere and contribute to producing renewable fuels as a feedstock for other processes [2].

Titanium dioxide (TiO_2) semiconductor material, among other metal oxide semiconductors, is a promising photocatalyst, has been consistently investigated, and has become a research hotspot for several photocatalytic applications [3]. Among the several benefits of using TiO_2, such as lower cost, higher stability, non-toxicity, and suitable oxidation band position, it has some limitations, such as being workable only under ultraviolet (UV) radiation and a higher charge recombination rate. Several strategies are used to increase TiO_2 photocatalytic efficiency through reducing charge carrier recombination, such as surface doping, modification, and constructing heterojunctions [4], [5]. For instance, when TiO_2 was combined with g-C_3N_4 and loaded with Ni active metal, more photocatalytic H_2 generation was achieved. [6]. Similarly, adding C/Ag to TiO_2 significantly improved CO_2 conversion to CO and CH_4, with a higher molar ratio obtained [7]. In many other reports, TiO_2 photocatalytic activity was increased by coupling with other semiconductors or loading with metals such as HCN/TiO_2 [8], La-C/TiO_2 [9], Ni-MMT/TiO_2 [10], and

In_2O_3/TiO_2 [11], which were responsible for higher productivity under UV and visible light irradiations.

In recent developments, MXenes with the general formula $M_{n+1}X_n$, where M represents early transition metals and X for C or N, and n=1, 2, 3, with properties similar to graphene, have been proposed to work as cocatalysts with other materials for photocatalytic efficiency. MXenes exhibit exceptional photocatalytic properties due to their distinct 2D accordion-like structure, remarkable light absorption capacity, high chemical stability, and excellent electrical conductivity. Ti_3C_2 is the most studied and ancient MXene because of its excellent electrical conductivity and structural stability [12]. In this perspective, various Ti_3C_2-based composites such as Ru-Ti_3C_2/g-C_3N_4 [13] and TiO_2/Ti_3C_2 [14] have been tested for various photocatalytic applications. Another intriguing substance is vanadium-based MXene (V_2C), which has drawn attention lately for several uses such as energy storage, catalysis, and photocatalysis. V_2C MXenes have good mechanical strength, high electrical conductivity, and excellent chemical stability. For instance, recently, we investigated V_2C potential as cocatalysts with g-C_3N_4 and found promising results for photocatalytic water splitting to produce hydrogen [15]. Another study investigated oxygen evolution processes by coupling V_2C-MXene with TiO_2 more efficiently [16]. In a different study, photothermal CO_2 reduction with Ni@NiO nanosheet-assisted V_2C composite was evaluated, with the possible production of CH_4 during the CO_2 methanation reaction [16]. On the other hand, little research has been done on using V_2C as a cocatalyst with TiO_2 for photocatalytic CO_2 reduction applications. Thus, utilizing 2D V_2C MXene as a cocatalyst with TiO_2 would be promising in maximizing the photocatalytic efficiency for CO_2 reduction in valuable products.

This work has studied using 2D V_2C MXene in conjunction with TiO_2 to produce V_2C-TiO_2 composite for photocatalytic CO_2 reduction applications. The process of CO_2 reduction was conducted with water as the reducing agent over the V_2C-TiO_2 composite, which resulted in the production of CO and CH_4. The V_2C-TiO_2 composite was synthesized using a self-assembly technique, whereas V_2C was produced through an HF etching procedure.

2. Experimental

2.1. Synthesis of Vanadium Carbide

2D structured vanadium carbide (V_2CTx) MXenes were produced by wet chemical etching of vanadium aluminium carbide (V_2AlC), as shown in Fig. 1 and according to our previous work [15]. 40 mL of 49% hydrogen fluoride and 1 g of V_2AlC MAX were mixed in a Teflon-lined reactor (HF). The mixture was left to stir at room temperature for 24 hours. After that, the suspension was centrifuged and washed multiple times with deionized water until the pH increased over 6.5. After that, V_2C MXene, the end product, was dried for an entire night at 100 °C in an oven. Safety precautions must be strictly followed when handling hydrofluoric acid (HF). Using HF-resistant gloves and preparing samples in a fume hood under controlled conditions is recommended. Before washing samples, HF should be separated and collected in a designated container for disposal, adhering to all established safety protocols.

Figure 1. Synthesis of 2D V_2C MXene through the HF etching method.

2.2. Synthesis of V_2C Supported TiO_2 Composite

The V_2C/TiO_2 nanocomposite was synthesized using a simple physical mixing approach as discussed in our previous work [17]. Typically, 500 mg of TiO_2 was dispersed in 20 mL of propanol and mixed for two hours. In parallel, while stirring the suspension above, a specific amount of V_2C dispersed in propanol was added. After stirring the mixture for 4 hours, it was dried at 100 degrees Celsius in an oven. By employing a similar approach, various V_2C-TiO_2 composite was synthesized using 25, 50, and 75 mg of V_2C MXene and designated 5V_2C-TiO_2, 10V_2C-TiO_2, and 15V_2C-TiO_2, respectively. The schematic depiction of the synthesis of V_2C-TiO_2 nanocomposites is shown in Fig. 2.

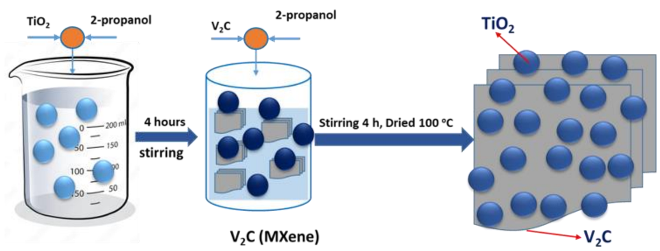

Figure 2. Synthesis of V_2C-TiO_2 composite through self-assembly approach.

2.3. Characterization of Materials

2.3.1 XRD analysis

The crystal structure of the catalyst was determined using X-ray diffraction (XRD) analysis, which provides detailed information about the material's phase composition and crystallinity. The measurements were carried out on a Rigaku Smart Lab diffractometer equipped with a Cu-Kα radiation source, operating at a wavelength of 0.15406 nm. The X-ray tube was set to a voltage of 40 kV and a current of 30 mA to generate the radiation required for diffraction. The sample was carefully prepared for the analysis by grinding it into a fine powder to ensure homogeneity. The powdered sample was then evenly spread onto a flat sample holder to facilitate accurate diffraction measurements. The XRD patterns were collected over a suitable 2θ range (e.g., 10° to 80°) with an appropriate step size and scanning speed to capture high-resolution data.

2.3.2 UV-visible analysis

The optical properties of the pure and composite materials were evaluated by acquiring their UV-visible diffuse reflectance (UV-Vis DR) absorption spectra using an Agilent Cary 100 spectrophotometer. Before measurement, the powder samples were carefully loaded into the instrument's integrating sphere to ensure uniform scattering and accurate reflectance data. The spectrophotometer was calibrated by performing a baseline correction. This was achieved by scanning the integrating sphere without any sample over the 200 to 1000 nm wavelength range to eliminate background noise and set the baseline to zero. Following baseline correction, the spectra of the samples were recorded under the same conditions. The instrument's settings, including scanning speed and resolution, were adjusted to optimize data quality and resolution.

2.3.3. Scanning electron microscopy (SEM) analysis

Scanning electron microscopy (SEM) analysis was conducted using a Hitachi SU8020 field emission scanning electron microscope (FESEM) to investigate the material's morphology and structural features. Before imaging, the samples were prepared by carefully dispersing fine particles of the material onto a carbon tape mounted on an aluminum sample holder. The samples were coated with a thin layer of gold to prevent charging effects during analysis using a sputter coater. The operating conditions, such as accelerating voltage and working distance, were optimized to achieve high-resolution images.

2.4. Photocatalytic Activity Test

A fixed-bed photoreactor was used to assess the performance of the photocatalytic system as reported in our previous work [18]. This system comprises an online product analysis system, light fixtures with cooling fans, and mass flow controls (MFC). A 200 W Hg bulb provides illumination in the UV range. A water saturator facilitates the transfer of CO_2 and water vapor into the reactor. To be more precise, the bottom surface of the reactor was filled with 150 mg of catalyst powder and was equally distributed. Before testing, the catalyst surface was saturated for thirty minutes by constantly running a mixture of CO_2 and H_2O through the reactor. All the experiments were conducted in a continuous flow mode in which the feed mixture was constantly flowing through the reactor during the experiments. The product was examined using gas chromatography with Thermal Conductivity Detector (TCD) and Flame Ionization Detector (FID) systems.

3. Results and Discussion

3.1. Characterization of Materials

Fig. 3 (a) shows the results of the XRD examination for the V_2C and V_2C-TiO_2 composite samples. Al atoms were extracted from their MAX phase to construct V_2C MXene successfully. The V_2C was indicated by basal planes (0 0 2) and (0 0 6) with 2θ of 13.29 ° and 41.24 °, respectively, and previously reported similarly [19]. The layered structure of V_2X MXene was responsible for the major peak, which was detected at 2θ of 41.24 °. In the literature, when 24 hours of etching of V_2AlC MAX powder with HF solution was conducted, V_2C MXene was produced [20]. All these results show successful synthesis of V_2C/TiO_2 composite without the presence of the impurity, and it would be beneficial to maximize the photocatalytic activity.

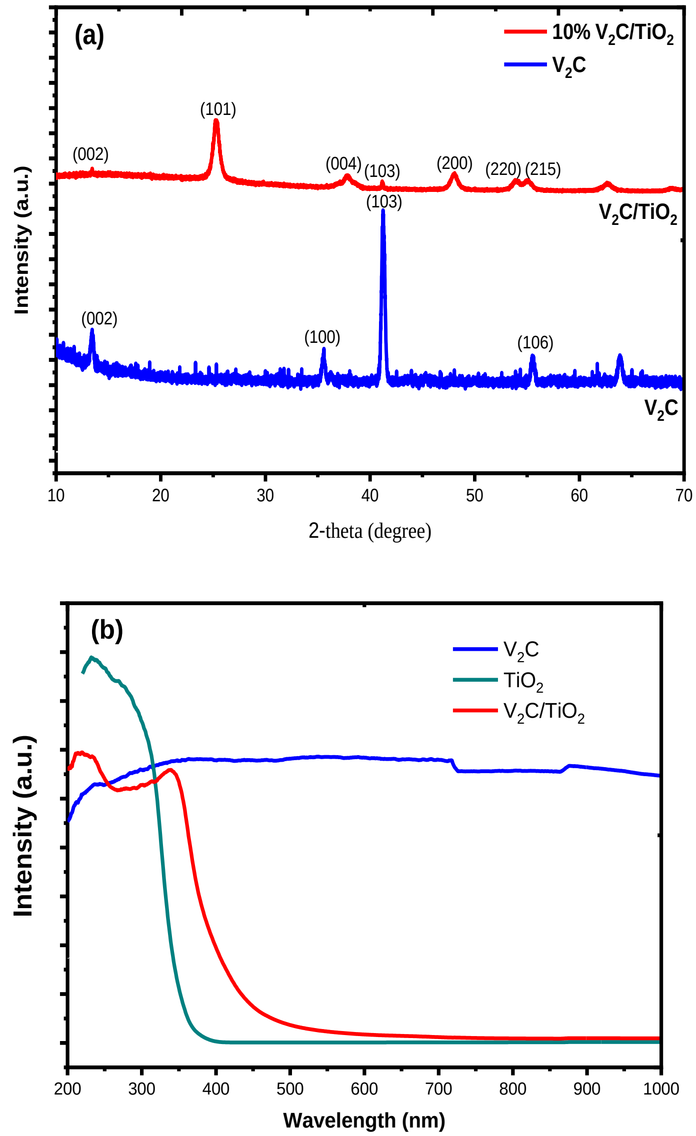

Figure 3. (a) XRD analysis of V_2C and V_2C-TiO_2 composites, (b) UV-visible analysis of V_2C and V_2C-TiO_2.

To learn more about the visible light absorption capacities of V_2C, TiO_2, and V_2C-TiO_2 composites, UV-visible analysis was carried out, and the findings are displayed in Fig. 3 (b). Because of its conductive properties and blackish color, pure V_2C exhibits a more substantial light absorbance than TiO_2, which exhibits light absorbance in the UV area, and similar information has been reported in the literature [21]. The absorbance band edge of TiO_2 was shifted towards the visible area upon V_2C loading. Therefore, the absorption of visible light is improved when V_2C is added to TiO_2 to form a V_2C-TiO_2 composite, as reported in the literature [22]. In previous work, higher light absorbance was obtained when a V_2AlC was added to TiO_2 and g-C_3N_4 [17]. In another work, when V_2C was added to V_2O_5/TiO_2, a decrease in band gap energy was obtained [23].

The FESEM examination of the TiO_2, V_2AlC, V_2C MXenes, and V_2C-TiO_2 composite is displayed in Fig. 4. TiO_2 nanoparticles with a consistent size and shape are seen in Fig. 4(a). The bulk phase of V_2AlC is depicted in Fig. 4(b) when all the layers are stacked with one another, with no interlayer gap. After the HF etching of V_2AlC MAX, a distinct gap between the layers was observed in V_2C MXene [24]. Fig. 4(c-d) depicts the morphology of the V_2C-TiO_2 composite, whereby TiO_2 particles are evenly dispersed across V_2C MXene to generate a favorable interface contact. These results show that V_2C-TiO_2 composites may be synthesized effectively and have potential applications in photocatalytic CO_2 reduction.

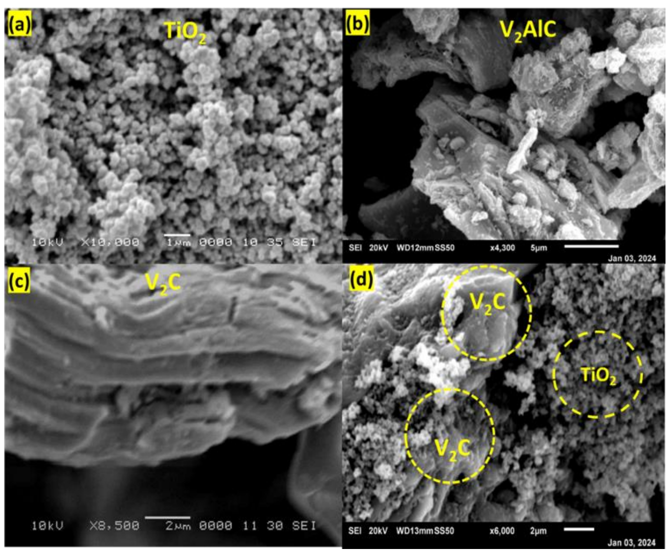

Figure 4. FESEM analysis (a) TiO_2, (b) V_2AlC, (c) V_2C, (d) V_2C-TiO_2 composite.

3.2. Photocatalytic Carbon Dioxide Reduction

To ensure that all of the photocatalyst samples were pure and that no products were produced from the carbon inside the photocatalysts, blank photocatalytic experiments were first carried out. This was accomplished by conducting three control experiments: one in which the photocatalyst and light source were used in an inert atmosphere without a feed mixture; another in which the photocatalyst and feed mixture were used but the light source was absent; and a third in which the photocatalyst and feed mixture were combined with the light source. These early experiments produced no CO or CH_4 compounds. This demonstrates that CO and CH_4 were only produced when the process took place under light irradiation and in the presence of both photocatalysts and the feed, and it validates the purity of the catalyst for photocatalytic CO_2 reduction.

Furthermore, all the data presented in this manuscript represent the average results obtained from multiple independent experiments. To ensure the reproducibility and reliability of the findings, each experiment was repeated at least three times under identical conditions. The experimental error was determined to be within a range of 5% to 10%. Notably, higher errors were observed for the pure samples, attributed to their lower measurement values and increased sensitivity to minor variations. In contrast, the composite samples exhibited reduced error margins, likely due to their enhanced stability and consistent properties. The observed errors are considered reasonable and are primarily attributed to the inherent variability associated with the batch processing of materials and the manual injection of samples during experimental procedures. These factors were carefully monitored and controlled to minimize their impact on the accuracy of the reported data.

In a fixed bed photoreactor system, Fig. 5(a) illustrates the performance of TiO_2 and V_2C loaded (5 to 15%) TiO_2 composites for photocatalytic CO_2 reduction with H_2O to produce CO and CH_4 under UV-light irradiation. CO was the primary product of the photocatalytic reduction of CO_2 with H_2O, using all pure and composite materials. Pure TiO_2 produced a lower rate of CO because of charges recombining along its surface during the irradiation period. However, when V_2C and TiO_2 were combined, photocatalytic efficiency significantly increased.

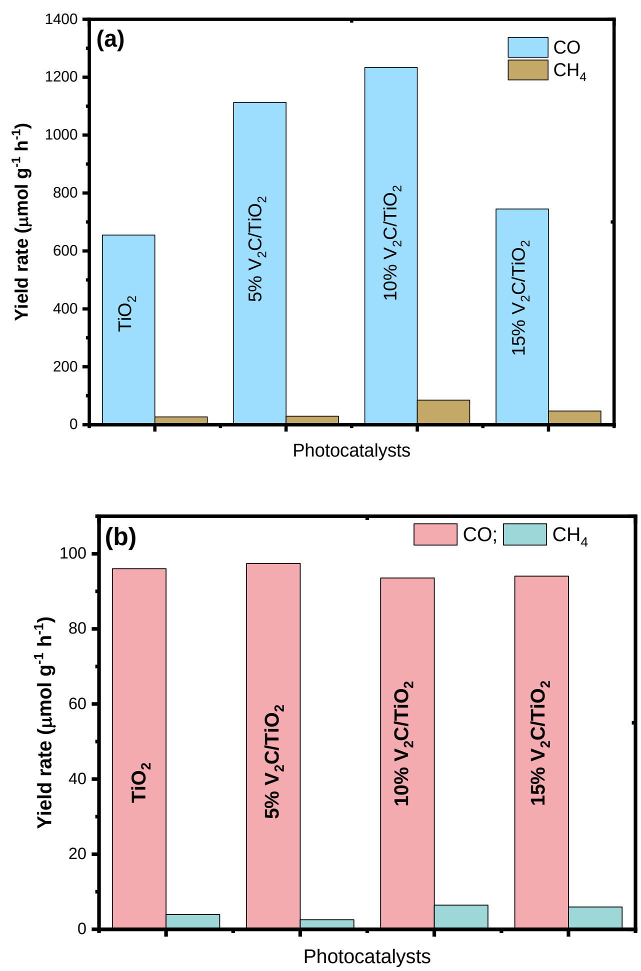

Figure 5. Photocatalytic CO_2 reduction with H_2O over various V_2C-TiO_2 composites: (a) CO and CH_4 formation, (b) performance analysis for selective CO and CH_4 formation.

After two hours of radiation, the CO yield rate was 654.77 μmol g^{-1} h^{-1}; when 5% V_2C was added to TiO_2, the rate rose to 1113.13 μmol g^{-1} h^{-1}. Conversely, when 10% V_2C was mixed with TiO_2, the highest CO generation was achieved, yielding a rate of 1233.84 μmol g^{-1} h^{-1}. The amount of CO generation with 10% V_2C-TiO_2 composite was 1.7 and 1.9 times greater, respectively, than with 5%V_2C-TiO_2 and pure TiO_2 samples. The reasons for the enhanced CO production photocatalytic activity were increased light irradiation utilization and efficient charge carrier separation.

In previous studies, the V_2C/TiO_2 composite demonstrated significantly higher hydrogen production, attributed to the efficient generation and separation of charge carriers facilitated by the presence of V_2C. This enhanced performance can be ascribed to the superior conductive properties of V_2C MXene, which promote effective charge transfer and reduce recombination rates. The excellent electrical conductivity of V_2C enables rapid electron transport, thereby improving the overall efficiency of the photocatalytic process and enhancing hydrogen evolution [25].

As previously mentioned, V_2C-TiO_2 composite samples have a greater capacity for charge creation and separation, which makes photocatalysis more effective at converting CO_2 to CO [21]. However, any increase in V_2C loading to TiO_2 led to decreased photocatalytic effectiveness, which may have been brought on by the composite structure's charge recombination centers and shielding effects [26]. In several other reports, similar observations have been reported. In our previous work, we tested Ti_2C_2/g-C_3N_4, and the optimized Ti_3C_2 loading of 10 % was obtained, in which the highest hydrogen production was obtained [13].

Fig. 5 (a) also displays the outcomes of photocatalytic CO_2 reduction to CH_4 over TiO_2 and V_2C-TiO_2 composites. The results for CH_4 production are similar to the evolution of CO when the production rate is decreased. With a 27.1 μmol g^{-1} h^{-1} rate, the CH_4 generation rate in V_2C-TiO_2 composite samples was much higher than that of pure TiO_2. With 10% V_2C-TiO_2 composites, the greatest CH_4 production of 85.2 μmol g^{-1} h^{-1} was attained. Compared to employing 15% V_2C and pure TiO_2 samples, this CH_4 production is 1.8 and 3.12 times more. Compared to pure TiO_2, the photocatalytic CO_2 reduction to CH_4 increased in the presence of V_2C because of the greater exposed surface area and effective charge carrier separation. In a recent study, Ag-NPs/V_2CT_x was found to have much improved water-splitting efficiency due to its lower charge recombination [27].

Fig. 5 (b) shows the CO and CH_4 generation selectivity over pure TiO_2 and V_2C-TiO_2 composite samples. CO selectivity of 96.04% was measured using TiO_2. The 10% V_2C-TiO_2 composite reduced somewhat to 93.60% but increased with 5% and 15% V_2C loading. This demonstrates that all photocatalysts were selective for CO2 reduction under UV light irradiation. Conversely, reduced CH_4 generation relative to CO could be caused by differences in electron production and redox potentials. It takes two electrons to generate CO, but eight electrons to form CH_4. It takes two electrons to generate CO, but eight electrons to form CH_4. Thus, the V_2C MXene sheets' conductive properties promote efficient electron transfer, which raises photocatalytic efficiency [28]. These characteristics support the notion that the well-designed V_2C-TiO_2 may be a potential non-noble photocatalyst for photocatalytic CO_2 reduction applications.

The performance of the current work was further compared with the similar work reported in the literature. In a recent work, when V_2C MXene was coupled with $LaCoO_3$/g-C_3N_4 and was tested for photocatalytic CO_2 reduction with H_2O, a CH_4 and CO yield rates of 332 and 171 μmol g^{-1} h^{-1} and their selectivity of 34% and 66%, respectively, were obtained [29]. The results reported in this work for CO and CH_4 production are lower than those of V_2C-TiO_2. However, a higher production of CH_4 was obtained. In another work, V_2AlC MAX/g-C_3N_4 was tested for photocatalytic dry reforming of methane and CO and H_2 evolution rates of 118.74 and 89.52 μmole g^{-1} h^{-1} with their selectivity of 57.01 and 42.98%, respectively [30]. All these findings confirm that V_2C-TiO_2 is a promising composite for the selective production of CO, which can be further used to produce various useful products.

Fig. 6 illustrates the mechanism of photocatalytic CO_2 reduction with H_2O to create CO and CH_4 over V_2C-TiO_2 composite under UV light irradiation. Due to higher metallic conductivity, it traps electrons from the semiconductors because it forms a Schottky interface junction, resulting in efficient separation of photoinduced charge carriers.

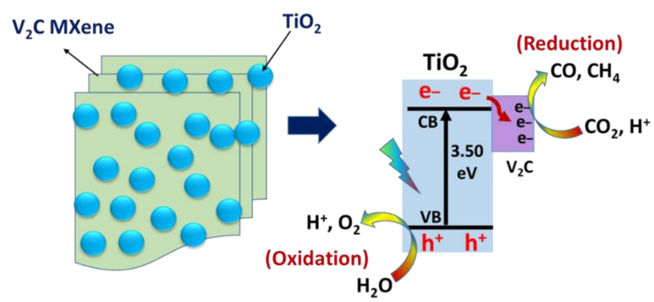

Figure 6. The schematic mechanism of producing CO and CH_4 through photocatalytic CO_2 reduction using H_2O over V_2C-TiO_2 composite under UV light irradiation.

Electrons and holes are produced over TiO_2 during the photocatalysis process, as shown in (1). TiO_2 CB electrons were moved to V_2C, capturing and moving electrons from TiO_2, as shown in (2). In previous work, when V_2C was coupled with g-C_3N_4, hindered charge recombination and their proficient separation were obtained during photocatalysis [15]. Equation (3) demonstrates the utilization of holes for water oxidation to produce protons and oxygen. According to the reaction in (5) – (6), protons and electrons were used to produce CO and CH_4, respectively [31], [32].

$$TiO_2 + light \xrightarrow{hv} e^- + h^+ \quad (1)$$

$$V_2C\,Mxene + e^- \longrightarrow V_2C(e^-) \quad (2)$$

$$H_2O + 2h^- \longrightarrow 2H^+ + 1/2O_2 \quad (3)$$

$$CO_2 + 2H^+ + 2e^- \longrightarrow CO + 2H_2O \quad (4)$$

$$CO + 6H^{+} + 6e^{-} \longrightarrow CH_4 + 2H_2O \quad (5)$$

According to experimental results, a higher amount of CO was produced than with the V_2C-TiO_2 composite. According to Equation (4), two electrons are required for CO production; however, as shown in Equation (5), CH_4 can only be produced with the availability of six electrons. This shows that initially, CO would be produced, which was further converted to CH_4 during the photocatalysis process. This higher CO production over the V_2C-TiO_2 composite would result from an efficient adsorption-desorption process and hindered charge recombination.

4. Conclusions

In conclusion, the photocatalytic CO_2 reduction process benefited from successfully fabricating V_2C MXene and V_2C-TiO_2 composite. Higher visible light absorbance was observed with V_2C and V_2C-TiO_2 composite, whereas effective charge carrier separation was caused by good surface interaction. During photocatalytic CO_2 reduction with H_2O, the main products obtained were CO and CH_4, whereas % 10%V_2C-TiO_2 composites yielded the highest production rate. Furthermore, the pure and composite materials showed selectivity for producing CO. V_2C MXene can be utilized as a co-catalyst with semiconductor materials to increase photocatalytic efficiency. The findings offer significant new data that could aid in photocatalyst research and design, increase process efficiency, such as CO_2 reduction, and promote sustainable technologies that support energy conservation and utilization.

Acknowledgements

This research was made possible through the financial support of the United Arab Emirates University (UAEU) under the research grant 12R212.

Conflicts of Interest

The authors declare no conflict of interest.

Author Contribution Statement

Beenish Tahir, Muhammad Tahir, and Abdulrahman Alraeesi: proposed the research problem, developed the theory and performed the computations, verified the analytical methods, and investigated

Beenish Tahir, Muhammad Tahir, and Abdulrahman Alraeesi verified the analytical methods and investigation.

Mustafa Jawad Nuhma and Ali A. Jazie: resources.

References

[1] M. Tahir and R. Mansoor, "Constructing Highly Stable CoAl-LDH-Coupled g-C_3N_4 2D/2D Heterojunctions for Solar Energy-Driven Conversion of Flared Gas to Syngas through Dry-/Bireforming of Methane," *Energy & Fuels*, vol. 37, no. 7, pp. 5241-5256, 2023, https://doi.org/10.1021/acs.energyfuels.2c03760.

[2] M. Yang *et al.*, "Atomic activation triggering selective photoreduction of CO_2 to CH_4 over NiAl-LDH/CeO_2 heterojunction," *Chem. Eng. J.*, vol. 472, 2023, https://doi.org/10.1016/j.cej.2023.145071.

[3] M. Tahir, B. Tahir, N. A. Saidina Amin, and H. Alias, "Selective photocatalytic reduction of CO_2 by H_2O/H_2 to CH_4 and CH_3OH over Cu-promoted In_2O_3/TiO_2 nanocatalyst," *Appl. Surf. Sci.*, vol. 389, pp. 46-55, 2016, https://doi.org/10.1016/j.apsusc.2016.06.155.

[4] M. Tahir, B. Tahir, N. A. S. Amin, and A. Muhammad, "Photocatalytic CO_2 methanation over NiO/In_2O_3 promoted TiO_2 nanocatalysts using H_2O and/or H_2 reductants," *Energy Conversion and Management*, vol. 119, pp. 368-378, 2016, https://doi.org/10.1016/j.enconman.2016.04.057.

[5] C. Yavuz and S. E. Ela, "Fabrication of g-C_3N_4-reinforced CdS nanosphere-decorated TiO_2 nanotablet composite material for photocatalytic hydrogen production and dye-sensitized solar cell application," *J. Alloys Compd.*, vol. 936, p. 168209, 2023, https://doi.org/10.1016/j.jallcom.2022.168209.

[6] S. Yang, K. Wang, Q. Chen, and Y. Wu, "Enhanced photocatalytic hydrogen production of S-scheme TiO_2/g-C_3N_4 heterojunction loaded with single-atom Ni," *J. Mater. Sci. Technol.*, vol. 175, pp. 104-114, 2024, https://doi.org/10.1016/j.jmst.2023.07.044.

[7] B. Yuan, H. Qian, Z. Luo, R. Zhu, and W. Luan, "A green synthetic approach for C/Ag@ urchin-like TiO_2 nanocomposites showing a highly molar ratio CH_4/CO for CO_2 photoreduction," *Materials Letters*, vol. 349, p. 134758, 2023, https://doi.org/10.1016/j.matlet.2023.134758.

[8] M. Tahir, "Investigating the Influential Effect of Etchant Time in Constructing 2D/2D HCN/MXene Heterojunction with Controlled Growth of TiO_2 NPs for Stimulating Photocatalytic H_2 Production," *Energy & Fuels*, vol. 35, no. 8, pp. 6807-6822, 2021, https://doi.org/10.1021/acs.energyfuels.1c00204.

[9] M. Tahir, "Hierarchical 3D VO_2/ZnV_2O_4 microspheres as an excellent visible light photocatalyst for CO_2 reduction to solar fuels," *Appl. Surf. Sci.*, vol. 467-468, pp. 1170-1180, 2019, https://doi.org/10.1016/j.apsusc.2018.10.273.

[10] M. Tahir, B. Tahir, Z. Y. Zakaria, and A. Muhammad, "Enhanced photocatalytic carbon dioxide reforming of methane to fuels over nickel and montmorillonite supported TiO_2 nanocomposite under UV-light using monolith photoreactor," *J. Cleaner Prod.*, vol. 213, pp. 451-461, 2019, https://doi.org/10.1016/j.jclepro.2018.12.169.

[11] Y. Wang *et al.*, "MIL-68 (In)-derived In_2O_3@TiO_2 S-scheme heterojunction with hierarchical hollow structure for selective photoconversion of CO_2 to hydrocarbon fuels," *Fuel*, vol. 331, p. 125719, 2023, https://doi.org/10.1016/j.fuel.2022.125719.

[12] A. Y. Zerga, M. Tahir, H. Alias, and N. Kumar, "Titanium Carbide MXenes Cocatalyst with Graphitic Carbon Nitride for Photocatalytic H_2 Production, CO_2 Reduction, and Reforming Applications: A Review on Fundamentals and Recent Advances," *Energy & Fuels*, vol. 37, no. 17, pp. 12623-12664, 2023, https://doi.org/10.1021/acs.energyfuels.3c01887.

[13] M. Tahir, "Nanoconfined Ti_3C_2@in-situ-grown TiO_2 and ruthenium triphenylphosphine (Ru-II) coupled g-C_3N_4 to construct RuP-Ti_3C_2@TiO_2/EC_3N_4 dual function nanocomposite for enhancing photocatalytic green hydrogen production," *Chem. Eng. J.*, vol. 476, p. 146680, 2023, https://doi.org/10.1016/j.cej.2023.146680.

[14] Y. Xu *et al.*, "In situ grown two-dimensional TiO_2/Ti_3CN MXene heterojunction rich in Ti^{3+} species for highly efficient photoelectrocatalytic CO_2 reduction," *Chem. Eng. J.*, vol. 452, 2023, https://doi.org/10.1016/j.cej.2022.139392.

[15] A. Sherryna, M. Tahir, and Z. Y. Zakaria, "Well-structured V_2C MXenes coupled g-C_3N_4 2D/2D nanohybrids for proficient charge separation with the role of triethanolamine (TEOA) as a protective barrier of g-C_3N_4 for stimulating photocatalytic H_2 production," *Int. J. Hydrogen Energy*, vol. 51, pp. 1511-1531, 2024, https://doi.org/10.1016/j.ijhydene.2023.09.234.

[16] F. Zhang, X. Zhang, S. Hu, H. Hu, J. Ye, and D. Wang, "Selective photothermal reduction of CO_2 to CH_4 via the synergistic effect of Ni-nanoparticle@NiO-nanosheet/V_2C-MXene catalyst," *Materials Today Energy*, vol. 39, 2024, https://doi.org/10.1016/j.mtener.2023.101470.

[17] M. Tahir, "Well-designed V2AlC MAX supported g-C3N4/TiO2 Z-scheme heterojunction for photocatalytic CO2 reduction through bi-reforming to produce CO and CH4," *Energy*, vol. 310, 2024, https://doi.org/10.1016/j.energy.2024.133231.

[18] B. Tahir, M. Tahir, N. Kumar, M. Siraj, and A. Fatehmulla, "Template-free synthesis of hierarchical graphitic carbon nitride (H-gC_3N_4) embedded with NiO for water splitting and CO_2 reduction with the role of hole scavenger: A comparative investigation," *Materials Science in Semiconductor Processing*, vol. 178, p. 108379, 2024, https://doi.org/10.1016/j.mssp.2024.108379.

[19] M. Alhabeb *et al.*, "Guidelines for Synthesis and Processing of Two-Dimensional Titanium Carbide ($Ti_3C_2T_x$ MXene)," *Chem. Mater.*, vol. 29, no. 18, pp. 7633-7644, 2017, https://doi.org/10.1021/acs.chemmater.7b02847.

[20] J. Chen *et al.*, "Construction Strategy of VO_2@V_2C 1D/2D Heterostructure and Improvement of Zinc-Ion Diffusion Ability in VO_2 (B)," *ACS Appl Mater Interfaces*, vol. 14, no. 25, pp. 28760-28768, Jun 29 2022, https://doi.org/10.1021/acsami.2c03646.

[21] M. Tahir, "Vanadium Carbide (V_2CT_x) MXene-Supported Exfoliated g-C_3N_4 with the Role of Hole Scavenger as a Rapid Electron Transfer Channel for Enhancing Photocatalytic CO_2 Reduction to CO and CH_4," *Energy & Fuels*, vol. 37, no. 14, pp. 10615-10630, 2023, https://doi.org/10.1021/acs.energyfuels.3c01301.

[22] R. Zhao, J. Liu, Y. Nie, and H. Wang, "Bismuth oxide modified V_2C MXene as a Schottky catalyst with enhanced photocatalytic oxidation for photo-denitration activities," *Environ Technol*, vol. 45, no. 9, pp. 1748 -1759, Dec 6 2022, https://doi.org/10.1080/09593330.2022.2152736.

[23] M. Tahir, "Synergistic Effect of the V2CTx MXene@V2O5/TiO2 NP Composite for Stimulating Photocatalytic CO2 Reduction through Bireforming of Methanol to Produce CO and CH4," *Energy & Fuels*, vol. 38, no. 11, pp. 10183-10202, 2024, https://doi.org/10.1021/acs.energyfuels.3c05215.

[24] L. Tan *et al.*, "Dual conductive confinement effects on enhancing Li-ion storage of NaV_6O_{15}@VO_2(M)@V_2C heterojunction," *J. Alloys Compd.*, vol. 964, p. 171242, 2023, https://doi.org/10.1016/j.jallcom.2023.171242.

[25] A. Zaka, M. A. Mansoor, M. A. Asghar, A. Haider, and M. Iqbal, "V_2C MXene-TiO_2 nanocomposite as an efficient electrode material for oxygen evolution reaction (OER)," (in English), *Int. J. Hydrogen Energy*, vol. 48, no. 89, pp. 34599-34609, Nov 1 2023, https://doi.org/10.1016/j.ijhydene.2023.05.230.

[26] H. Gu *et al.*, "Robust construction of CdSe nanorods@Ti_3C_2 MXene nanosheet for superior photocatalytic H2 evolution," *Appl. Catal., B*, vol. 328, 2023, https://doi.org/10.1016/j.apcatb.2023.122537.

[27] Z. Haider *et al.*, "Ag Nanoparticle-Decorated V_2CT_x MXene Nanosheets as Catalysts for Water Splitting," *ACS Applied Nano Materials*, vol. 6, no. 4, pp. 2374-2384, 2023, https://doi.org/10.1021/acsanm.2c04428.

[28] S. Akir *et al.*, "Atomic-layered V_2C MXene containing bismuth elements: 2D/0D and 2D/2D nanoarchitectonics for hydrogen evolution and nitrogen reduction reaction," *Nanoscale*, vol. 15, no. 30, pp. 12648-12659, Aug 3 2023, https://doi.org/10.1039/d3nr01144e.

[29] M. O. Madi and M. Tahir, "Well-designed 2D vanadium carbide (V_2C) MXenes supported $LaCoO_3$/g-C_3N_4 heterojunction for highly efficient and stable photocatalytic CO_2 reduction to CO and CH_4," *J. Alloys Compd.*, vol. 983, 2024, https://doi.org/10.1016/j.jallcom.2024.173730.

[30] M. Madi and M. Tahir, "Fabricating V_2AlC/g-C_3N_4 nanocomposite with MAX as electron moderator for promoting photocatalytic CO_2-CH_4 reforming to CO /H_2," *International Journal of Energy Research*, pp. 1-20, 2022, https://doi.org/10.1002/er.7667.

[31] X. Wang, Z. Jiang, H. Chen, K. Wang, and X. Wang, "Photocatalytic CO_2 reduction with water vapor to CO and CH_4 in a recirculation reactor by Ag-Cu_2O/TiO_2 Z-scheme heterostructures," *J. Alloys Compd.*, vol. 896, p. 163030, 2022, https://doi.org/10.1016/j.jallcom.2021.163030.

[32] L. Wang *et al.*, "Preparation of CdS-P25/ZIF-67 composite material and its photocatalytic CO_2 reduction performance," *Appl. Surf. Sci.*, vol. 584, p. 152645, 2022, https://doi.org/10.1016/j.apsusc.2022.152645.